Chirped pulse amplification experiments on the VULCAN Nd:glass laser facility

C N Danson, L Barzanti, Z Chang‡, A Damerell, M D Dooley, C B Edwards, S Hancock, M H Key, R Mahadeo, M R G Miller, P Norreys, C E Ollman, D A Pepler, D A Rodkiss, I Ross, M A Smith, P F Taday, W T Toner, K Wigmore, T B Winstone, and R W W Wyatt
Central Laser Facility, Rutherford Appleton Laboratory, Chilton, Didcot, Oxon, UK.
‡ Visiting scientist to RAL from Xian Inst. of Optics and Precision Mechanics, People's Republic of China

S Luan, F Beg, A Bell, A E Dangor, M H R Hutchinson, P Lee, I P Mercer, R A Smith and F Zhou
Blackett Laboratory, Imperial College, Prince Consort Road, London, UK.

A P Fews
H H Wills Physics Laboratory, University of Bristol, Tynoal Avenue, Bristol, Avon, UK.

1. INTRODUCTION

A Chirped Pulse Amplification (CPA) mode of operation is being developed on the VULCAN high power Nd:glass laser system[1], at the Rutherford Appleton Laboratory (RAL). Experiments have been carried out using an interim configuration yielding pulses of up to 30 J on target of 2.4 picoseconds length at focused intensities up to 4×10^{17} W cm^{-2}, with contrast ratio of 10^6. Laser performance and preliminary plasma physics data are presented.

Picosecond pulses of high energy focused to ultra high intensities (> 10^{17} W cm^{-2}) are becoming increasingly important in laser-plasma interaction studies. Applications include recombination XUV lasers, beat-wave and Wakefield particle accelerators[2], high harmonic generation[3], multi-photon ionisation[4], solid density interactions[5] and improved temporal resolution of X-Ray backlighting[6] and optical probing diagnostics.

In the CPA technique[7,8] the amplification of a stretched pulse to high energy followed by recompression provides a means of delivering a higher peak power to target than can be propagated through the laser system due to non-linear effects and component damage thresholds. In the system described here a grating pair is used to stretch a transform limited pulse of 2 ps, to 80 ps prior to amplification to high energy (80 J). The linear stretch produced by the gratings enables the pulse to be recompressed without pedestal. Recompression to the 10 TW level by a second grating pair is carried out in a vacuum propagation and reflective focusing system to avoid non-linear effects in air, windows and lenses.

2. LASER CONFIGURATION

Figure 1 shows schematically how the CPA technique was implemented on VULCAN. An oscillator provided a CW train of low energy (< 1 nJ), 2 ps pulses. This pulse train was amplified in a double pass rod pre-amplifier, and a single pulse selected. This pulse was then stretched to ~80 ps in a double passed grating configuration before being injected into the high power Nd:phosphate glass amplifier chain of VULCAN. The output beam was ~135 mm in diameter and contained up to 80 J in energy. The beam was then re-compressed using a second pair of gratings to ~2 ps. For the experiments described the maximum energy on target was limited to 30 J because of grating inefficiencies and aperturing of the beam. The beam was focused using an off-axis parabola to avoid the non-linear effects associated with transmissive optics, to a focal spot size of ~50 μm and power densities of ~4×10^{17} W cm^{-2}.

2.1 Pulse generation

An Additive Pulse Modelocked (APM)[9,10] oscillator based on a Michelson configuration[11], was developed for this work. The oscillator employed Nd:YLF as the active medium and was pumped by a laser diode. Nd:YLF has been predominantly chosen as the gain medium for oscillators used with phosphate glass amplification

 0-8194-1087-X/93/$6.00

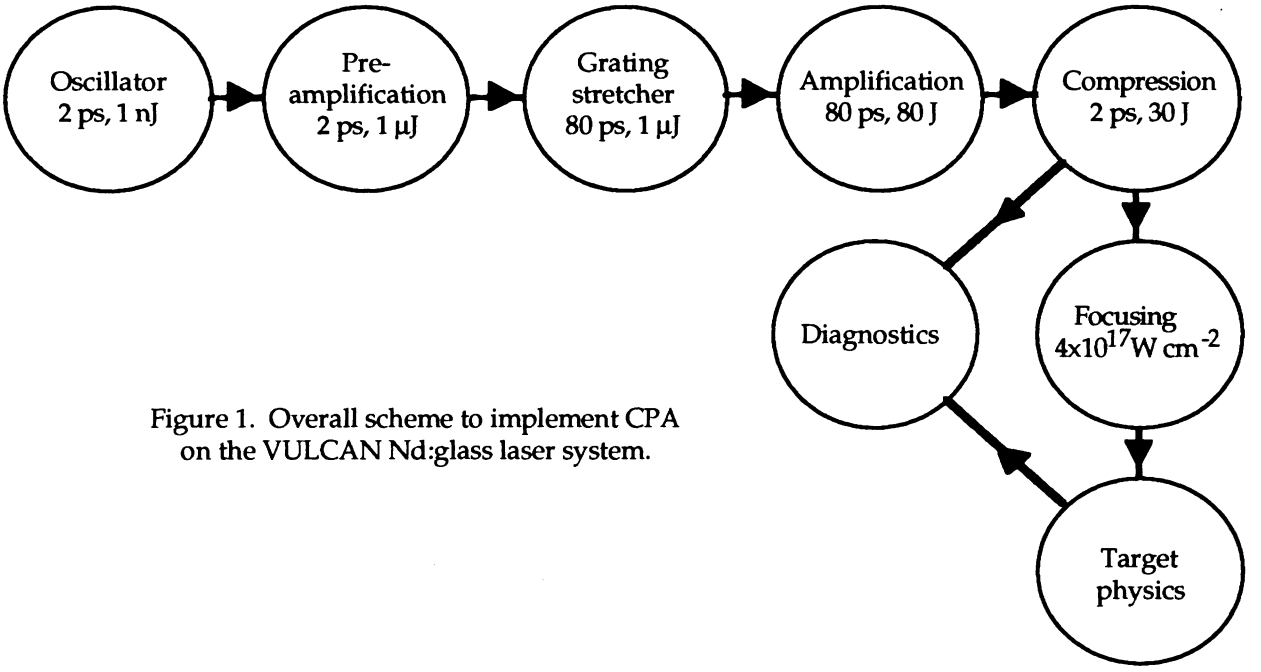

Figure 1. Overall scheme to implement CPA on the VULCAN Nd:glass laser system.

because of the close wavelength match to the peak of the phosphate gain (1053 nm), its high efficiency, large bandwidth, and good thermal properties. The large bandwidth (1.2 nm) supports the generation of picosecond pulses. It has strong absorption lines at 800 nm and so can be pumped efficiently by a GaAlAs diode laser.

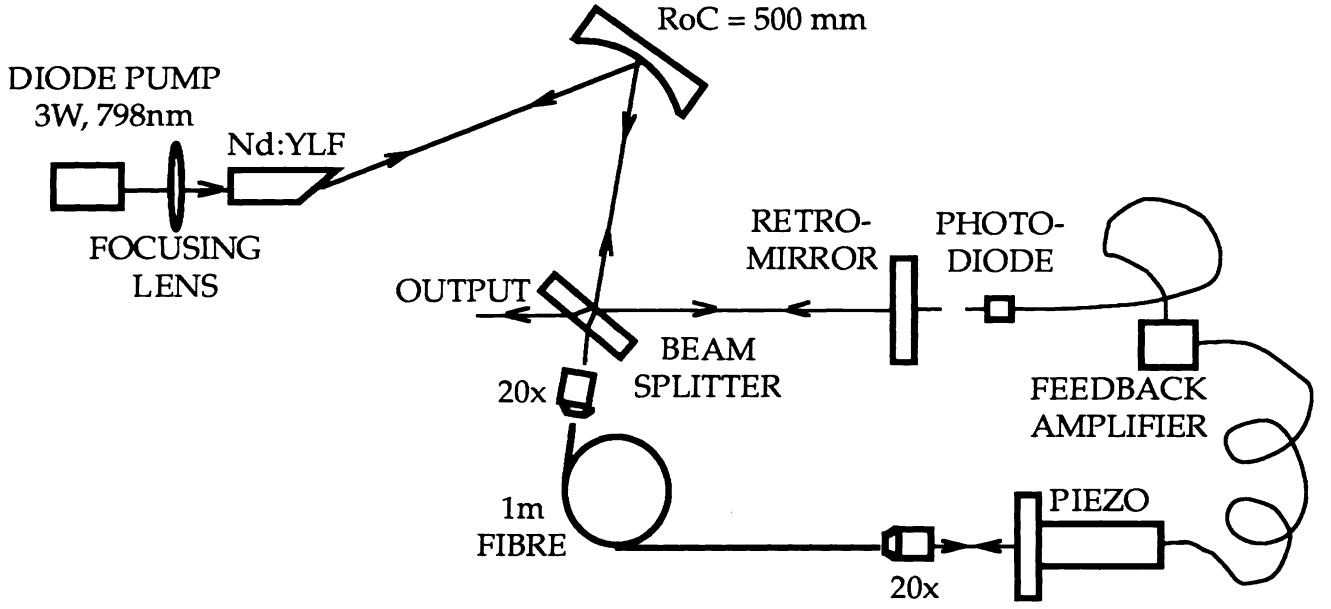

Figure 2. A schematic of the diode-pumped APM Nd:YLF oscillator using the Michelson configuration.

A schematic of the oscillator is shown in figure 2. The laser diode (SDL-2482-PI) was a 3 W gain guided, partially coherent, phase coupled, GaAlAs multi-stripe device. The output was coupled to a plano-Brewster Nd:YLF rod through a dichroic multi-layer dielectric coating, < 5% reflective at 800 nm and > 95% reflective at 1053 nm, on the plano surface. The coupling optics consisted of a high numerical aperture (0.65) multi-element collimator, a 100 mm focal length cylindrical lens to correct for the astigmatic output mode pattern of the diode array, a half-wave plate and a 25 mm focal length plano-aspheric focusing lens.

The oscillator consisted of two coupled cavities, corresponding to the two arms of a Michelson interferometer. The resonators consisted of four mirrors: the plano end of the Nd:YLF rod, the 500 mm ROC spherical mirror, the output coupler and the retro-reflectors. The spherical mirror produced a stable cavity and compensated for the astigmatism introduced by the Brewster angle of the rod. To achieve high efficiency the pumping mode in the rod must overlap with the laser mode. The size of the laser mode in the rod is dependent on the separation between the rod and the spherical mirror, while the output mode shape is dependent on the folding angle of the spherical mirror. In the configuration used the separation was 290 mm and the angle 30 degrees. The separation between the folding mirror and the output coupler was approximately 1 m.

A 1 m length of optical fibre was inserted into the non-linear cavity to generate chirp on the pulse through self-phase modulation. The non-linear cavity length was an integral multiple of the length of the linear cavity. When the two pulses from the two cavities interfere at the beam-splitter, the pulse duration is progressively reduced. This is due to phase differences between the leading and trailing edges, which when summed reduces their intensity.

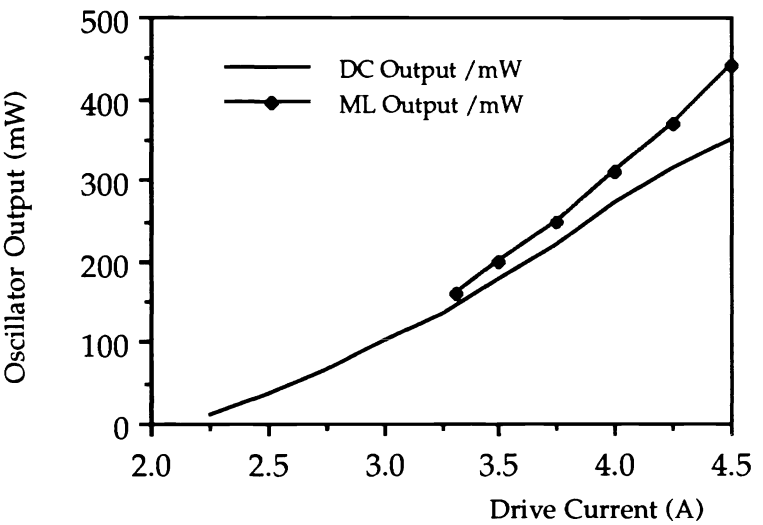

Figure 3. Output Power Characteristics of the Michelson APM Oscillator

The reflectivity of the beam-splitter was 90%, chosen as a compromise between high output power and low modelocking threshold. The output power characteristics from the oscillator are shown in figure 3. The maximum stable mode-locked output was 440 mW, and the shortest pulse duration obtained 1.68 ps (for a sech^2 pulse shape). It was found that the pulse duration changed with the pumping power and careful optimisation was required to achieve the minimum pulse duration. For a fixed pumping power, the pulse duration changes with the phase of the pulse from the non-linear cavity. This was adjusted by changing the offset of the feedback electronics to change the position of the mirror on the piezoelectric transducer.

The output power also changed with the phase, with the highest peak power corresponding to the shortest pulse duration for a given CW pumping power. The shortest pulse duration which could be produced ranged

from 1.68 - 1.90 ps, dependent on the length of fibre. The pulse width was extremely sensitive to the fibre coupling efficiency, but insensitive to the absolute fibre length, provided that it introduced sufficient self-phase modulation to the pulse. With the Michelson cavity configuration output pulse stability was maintained throughout the entire pumping range.

2.2 Pulse Amplification

The typical pulse energy from the oscillator ~1 nJ, significantly below (~10^{-4}) the normal input to the VULCAN amplifiers (~10 μJ). To achieve the 80 J system output required for the experiment, a double passed 9 mm diameter Nd:glass rod amplifier was used to pre-amplify the pulse. The gain of the pre-amplifier could be varied between 200 - 900, by adjusting the flashlamp drive voltage. A Faraday rotator provided the isolation between the oscillator and the pre-amplification system necessary to protect the oscillator from back-reflections, which could seriously affect mode-locking stability or damage components.

A single pulse was selected from the CW pulse train using two Pockel cells in series, giving an extinction ratio of > 10^5. After injection into the main system, a third Pockel cell was used in the small aperture rod amplification stage to improve the contrast to > 10^8. The gate widths for these cells were ~1 ns and ~10 ns respectively, sufficiently short to eliminate satellite pulses from the oscillator.

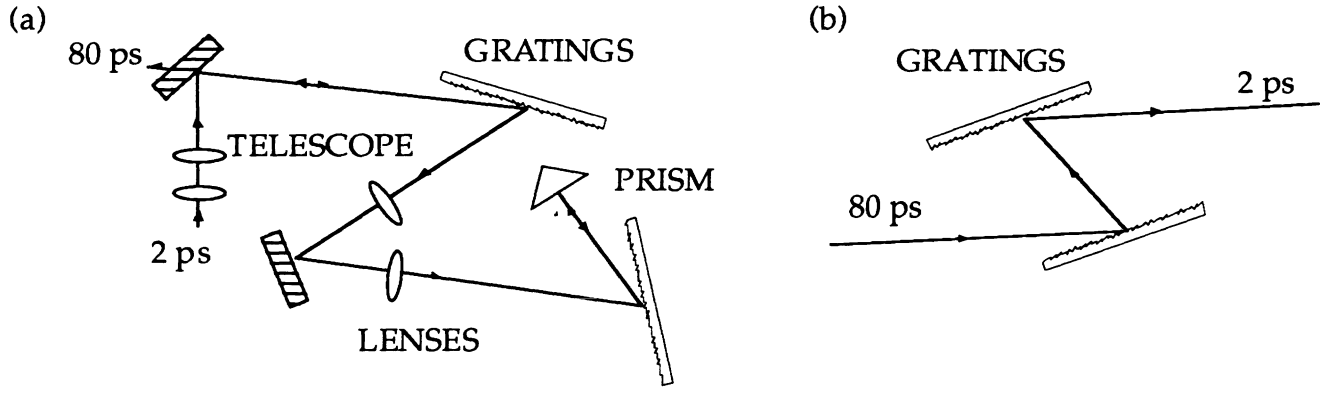

Figure 4. Schematics of the grating stretcher and compressor.

The pulse was stretched using a double passed grating pair, as shown in figure 4(a). The gratings introduce a frequency dependent time delay, producing a pulse with a linear frequency sweep (chirp). Holographic, gold coated gratings were chosen with 1740 lines/mm in a sinusoidal profile blazed for optimum efficiency at 1053 nm. They were operated at a diffraction angle (θ_d) of 61 degrees. The degree of stretching is given by [12,13]

$$\Delta\tau = \frac{4 l_{stretch} m^2 a^2 \lambda \Delta\lambda}{c \cos^3 \theta_d}$$

where: λ is the wavelength, $\Delta\lambda$ is the bandwidth of the pulse, m is the diffraction order, a is the grating line density, $l_{stretch}$ is the perpendicular distance from the grating to the focal point of the lens, c the velocity of light in vacuum, and $\Delta\tau$ is the stretched pulse-width.

The bandwidth of the oscillator pulse was ~0.60 nm giving a calculated stretched pulse duration of ~79 ps. Figure 5 shows a streak-camera image of the stretched pulse. The two pulses are present as a calibration of the measurement on every shot. The data gives a value of 80 ± 10 ps for the stretched pulse width in good agreement with the theoretical value.

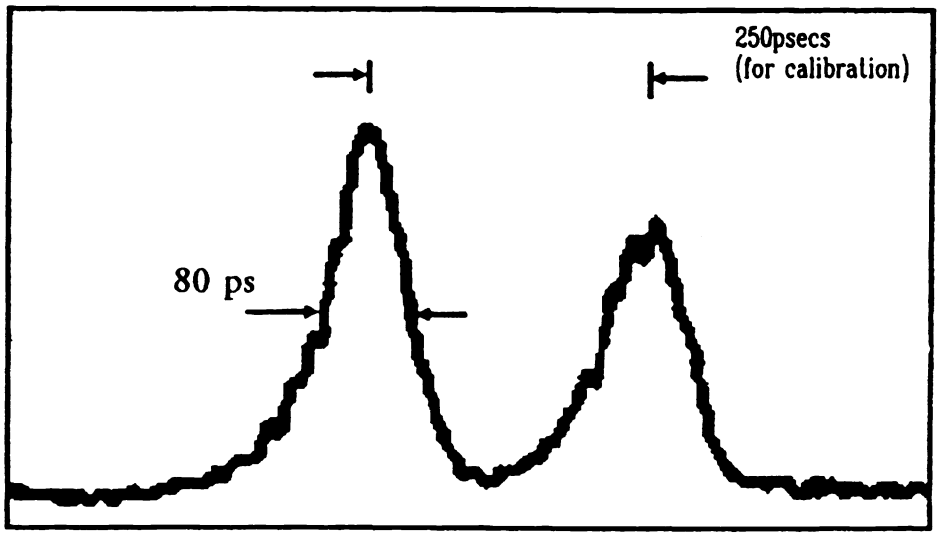

Figure 5. Streak camera image of the stretched pulse

The pulse was first amplified in a series of Nd:phosphate glass rods up to a diameter of 45 mm to give a pulse energy of up to 1 J. The beam was then expanded to 90 mm and passed through a double passed 108 mm diameter disc amplifier, and a 150 mm clear-aperture disc amplifier. With this configuration the total gross system gain was ~2 x 10^{14}. The injection and system losses were estimated at 10^4, giving a nett system gain of ~2 x 10^{10}. A maximum output energy of 80 J could be generated from the output amplifier, with a maximum of 30 J on to target, (allowing for grating efficiencies and other losses in the target area optics). The output energy was limited by the need to avoid optical damage at the stretched pulse width. Following the final 150 mm amplifier the beam was apertured horizontally to 88 mm to prevent clipping on the diffraction gratings. A soft aperture was used to minimise modulations in the near field which would damage the gratings. Aperturing was achieved using a pair of profiled linear edges with a repeated x^2 ($-1 < x < 1$) modulation, 3 mm in amplitude and with a period of 1 mm.

3. PULSE COMPRESSION

The amplified pulse was propagated to one of the VULCAN target areas which was reconfigured for these experiments. The pulse was then re-compressed using a single pass through a pair of large aperture diffraction gratings of a similar type to those used in the stretcher, but having a ruled area of 300 mm x 150 mm. To minimise non-linear effects due to propagation of high intensity laser pulses through air, the second grating was housed within an evacuated extension to the target chamber. A schematic of the grating and target chamber layout is shown in figure 6. At the input window the pulse length was ~40 ps. A photograph of the target area is shown in figure 7.

The duration of the re-compressed pulse was measured using a second-order single-shot auto-correlator[14]. The pulse length dependence on grating separation is shown in figure 8, with the minimum pulse duration being obtained with a grating separation of 2.78 m. The first grating was mounted on a 0.5 m long pneumatic slide which allowed the separation to be optimised.

3.1. Pulse width and energy

At high energies (greater than 10 J), it was found that as the energy in the pulse increased, the re-compressed pulse-width also increased. Due to B-integral effects producing self-phase modulation (SPM) on the stretched

Figure 6 Engineering drawing of the grating configuration and target chamber layout for the CPA experiments.

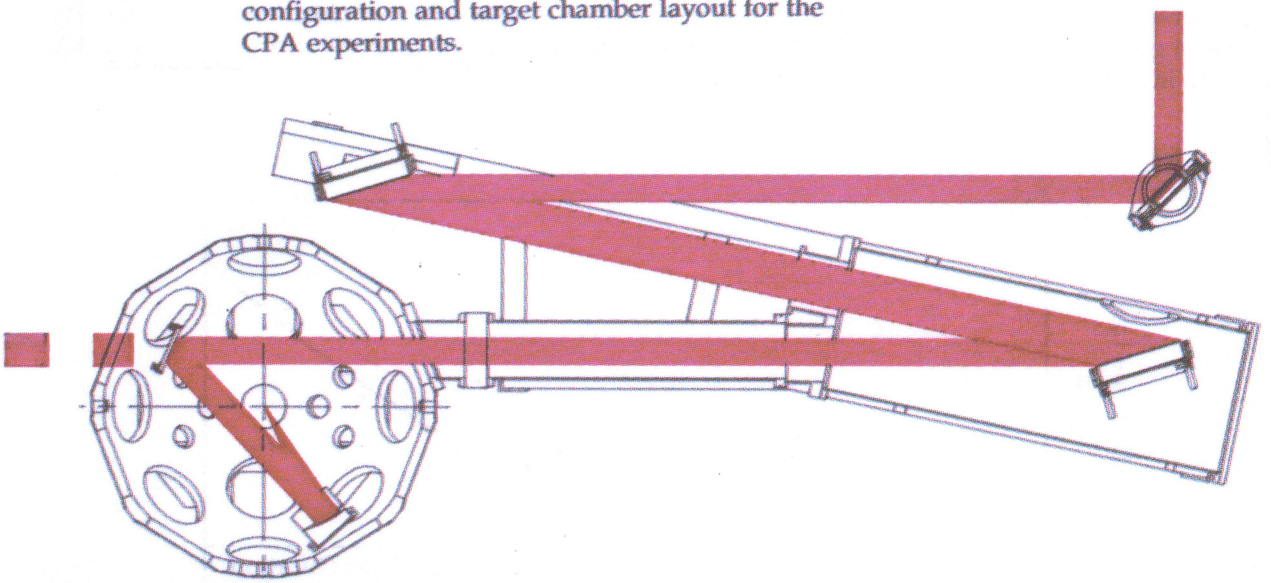

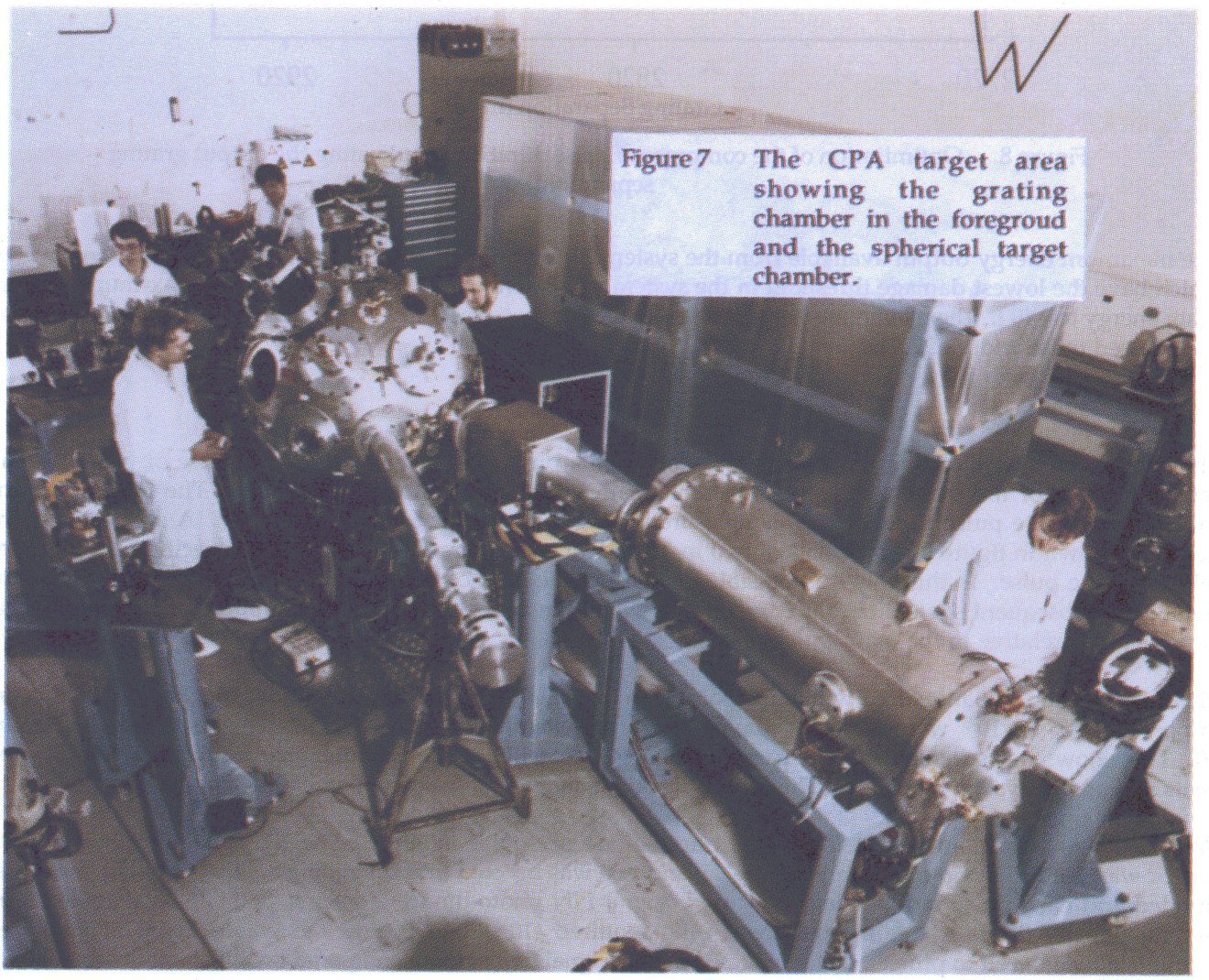

Figure 7 The CPA target area showing the grating chamber in the foregroud and the spherical target chamber.

pulse as it propagated through the system[15]. Having optimised the grating separation for a particular configuration at low energies, the extra SPM at higher energies causes a further chirp on the pulse, detuning the system and giving the longer pulse-widths. However, by reducing the B-integral during the experiment, it was possible to increase the threshold for the onset of pulse broadening to ~20 J.

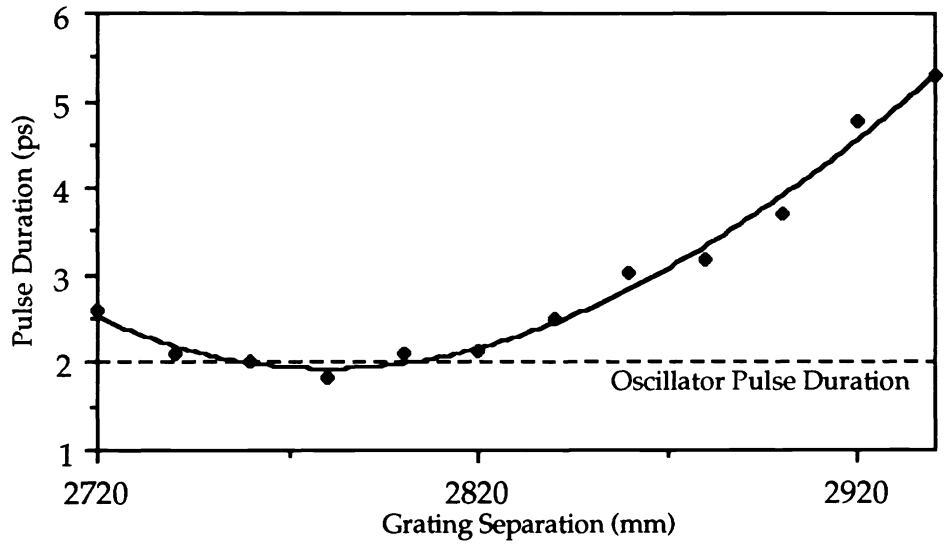

Figure 8. Optimisation of the compressed pulse duration by adjusting the output grating separation

The maximum energy output available from the system is determined by the damage threshold of the gratings which have the lowest damage threshold in the system, at ~300 mJ cm^{-2}. This restricted the maximum incident beam energy to ~40 J. The maximum measured power on to target was 8 TW produced from a 19 J shot, with a re-compressed pulse width of 2.4 ps.

3.2. Contrast ratio

The contrast of the pulse is an important issue for plasma physics experiments. A pre-pulse or pulse plateau causes preheat of the target producing a plasma with which the short pulse interacts. The contrast of the background of the pulse to its peak was measured using a third order cross-correlator[16]. A schematic of the device is shown in figure 9. It consists of two independent correlators that measure two specific points in time relative to the pulse. In this way it is possible to measure the peak of the pulse and a point in the wings of the pulse. On subsequent shots different points in the wings can be measured to give mapping of the pre-pulse at various times relative to the main pulse.

The contrast ratio was measured with a temporal scan from 600 ps before the main pulse to 200 ps after. No pre or post pulses > 5×10^{-5} were detected. The pulse profile generated from these measurements is shown in figure 10. This shows measurements of the pre-pulse using the oscillator output, after pre-amplification, using rod shots and on full system disc shots. The contrast ratio is consistently measured at > 10^{-6}.

Pre-pulse was also monitored using a PIN photo-diode pre-pulse monitor. The leakage through a steering mirror was used to sample the stretched pulse, and this was injected into the monitor. The sampled beam was divided and each pulse independently focused onto a PIN photo-diode. The first path was attenuated with neutral density filters to the measurement ratio required (10^{-4}), and the second was delayed and focused through a water cell to protect the sensor. The two signals were then compared on a fast oscilloscope at the

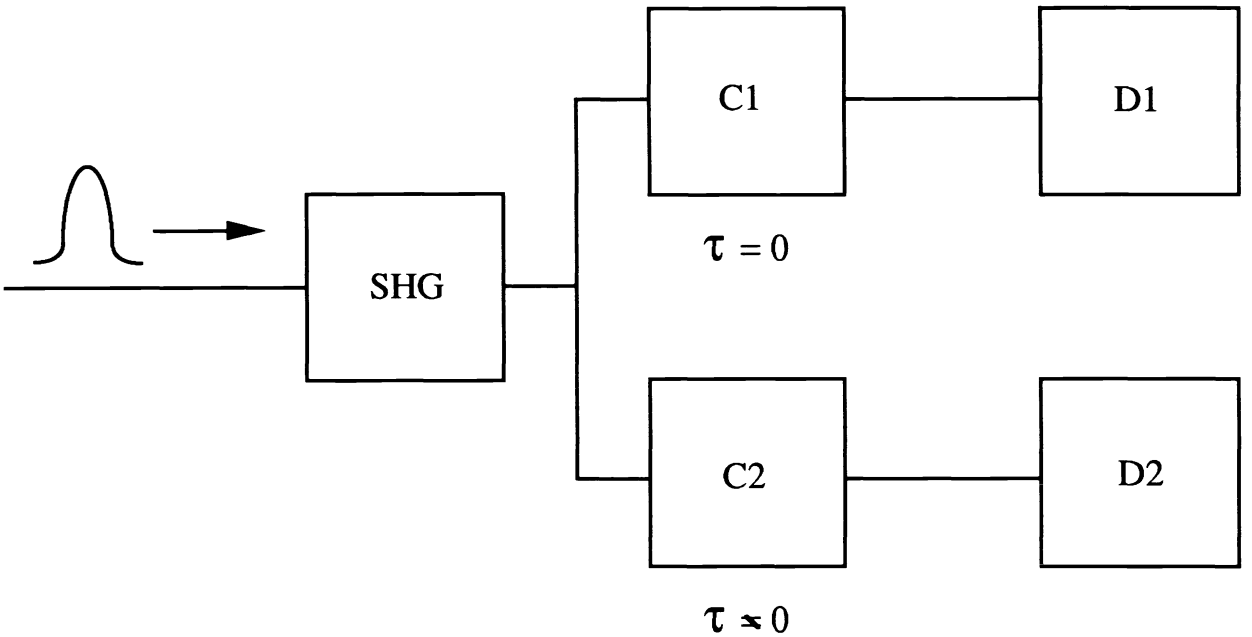

C1, C2 - CROSS CORRELATORS

D1, D2 - PHOTOMULTIPLIERS

Figure 9. Schematic of the Third Order Cross - Correlator for contrast measurements.

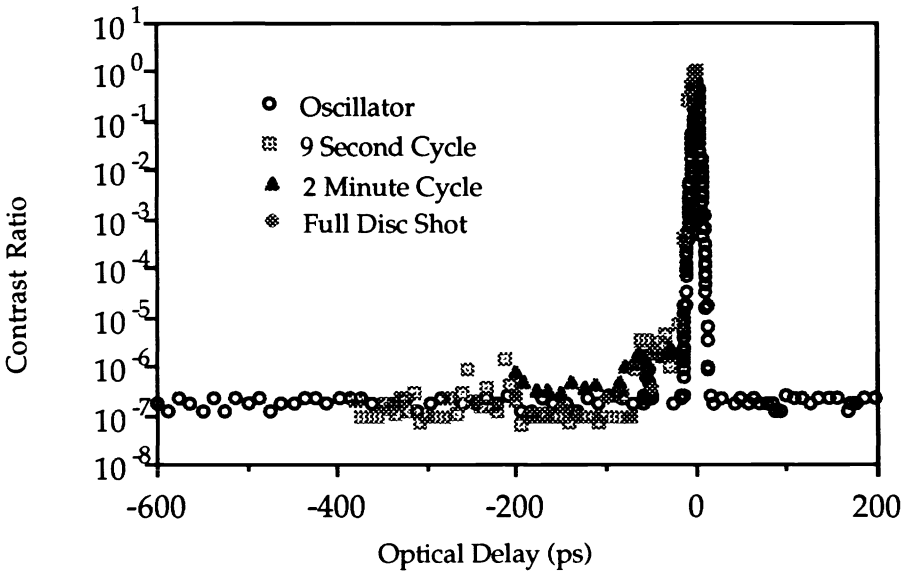

Figure 10. Contrast ratio measurement of the compressed pulse

same input sensitivity, so that the first pulse produced an intensity fiducial for the second. The use of PIN diodes gives the diagnostic a good sensitivity and the ability to be less sensitive to electrical noise. The filtering allows the measurement level to be easily chosen in the range 10^{-2} - 10^{-5}. For the experiment this detector was calibrated at the 10^{-4} level for a full scale deflection, which would still allow a pre-pulse of ~5 x 10^{-5} to be detected within a time window of some 30 ns, and with a resolution of about 500 ps. On pre-pulses were observed using this monitor.

4. BEAM FOCUSING

The beam was focused by an off-axis parabola onto target as shown in figure 6. The parabola had a clear aperture of 165 mm, a focal length of 448 mm and an off-axis distance of 110 mm. It was coated with a multi-layer dielectric to give > 99% reflectivity at 1053 nm. The residual beam passing through the 95% reflective steering mirror was used to provide the diagnostics with a sample of a pulse.

An equivalent-plane monitor was used to measure the far-field intensity distribution of the re-compressed pulse. The beam was focused through a 4.3 m lens, then passed through an etalon to produce an array of foci. Figure 11 shows the beam at best focus to be 5 - 10 x the diffraction limit.

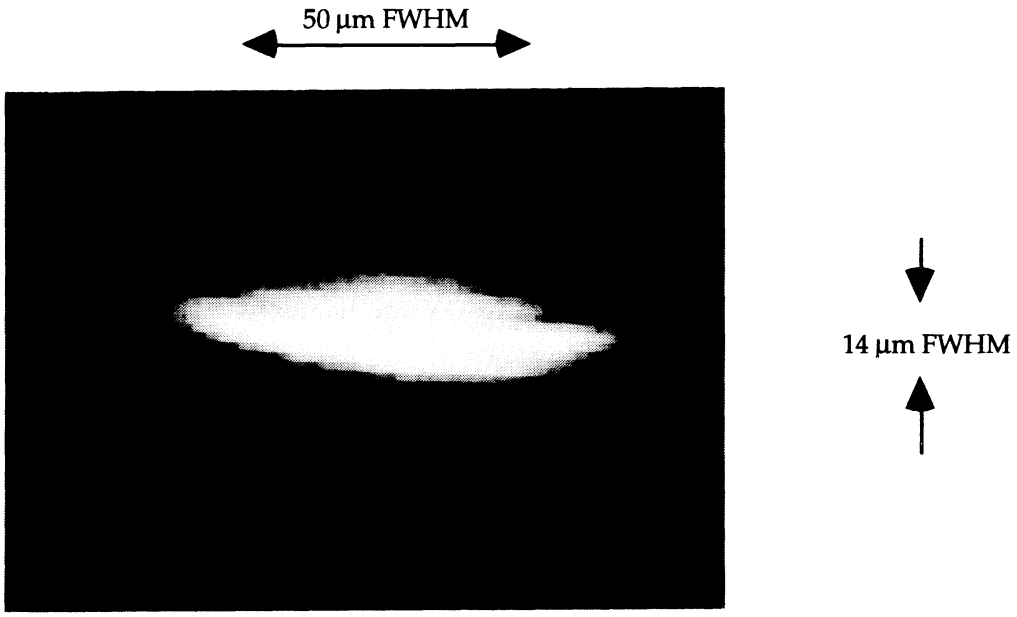

Figure 11. Equivalent plane image of the focal spot

To measure the energy contained within the focal spot a series of shots were taken, focusing the beam through a 100 μm pinhole in a 100 μm thick platinum substrate. The transmitted energy was measured with a calorimeter. The energy was varied from 6 J to 23 J to confirm that there was no significant beam degradation with increased energy. Each shot gave a pinhole transmission of 89%, giving a focal spot size of ~50 μm full width half maximum, assuming a gaussian profile.

The 50 μm focal spot size was confirmed by x-ray images obtained from two pinhole cameras monitoring x-ray generation from the plasma at energies ~ 25 keV.

5. TARGET PHYSICS

Laser-plasma interactions have been extensively studied under conditions where the laser pulse length is long enough to allow the hydrodynamic flow of the plasma to approach a steady state. Under these conditions heating occurs at densities close to the critical density. Few studies have been performed under conditions where the laser pulse is short compared with the hydrodynamic response time of the plasma and where the heating occurs close to solid density. Initial experiments were performed using the CPA operating mode of VULCAN to investigate laser-plasma interactions under such conditions. The target was placed at chamber center and rotated away from normal to the incident beam to minimise any back-scattered signal into the amplifier system. Diagnostics used included: x-ray pinhole cameras to image the plasma extension; Faraday cups to record the ion velocities up to 100 keV, CR39 nuclear plastic detectors measure ion velocities > 100 keV and two NaI-scintillator detectors to measure the hard x-ray emission.

In most of the high energy shots the plasma was confined into a collimated plume that was directed outward normal to the target surface. This effect was clearly seen with planar targets of mylar, carbon and copper. Evidence for plasma confinement was also obtained from the Faraday cup data. Four cups were placed in a vertical line from the target normal from 10° to 25°. It was found that the integrated energy flux was five times higher for the 10° cup than for the 25° cup.

The CR39 detectors showed that nearly all the fast ions incident on the target were protons that were associated with hydrocarbon contamination of the target surface. There was a peak in the distribution at 300 - 400 keV followed by an exponentially decaying tail up to 1.5 MeV. The energy absorbed by the proton with energies > 100 keV averaged 2% of the incident energy and was never higher than 5%. There was also an energy peak at ~30 keV / nucleon in the Faraday cup signal. It was found that 80% of the energy incident on a Faraday cup was associated with the fast ion feature. Hence if it is assumed that this 30 keV / nucleon feature can be associated with the carbon ions (the kinetic energy of these ions would also be 300 400 keV), then a quantitative estimate of the absorbed energy can be obtained by multiplying the total flux measured by the CR39 with the proportion of contaminant that was carbon to hydrogen (ie. 2 : 1 for CH_2).

The collimation of the plasma blow-off may be caused by large thermo-electric magnetic fields associated with the crossed density and temperature gradient. Two dimensional simulations support our observations and have also shown that the plasma blow-off is confined to a collimated plume. Detailed analysis of these results will be reported elsewhere[17].

6. CONCLUSION

A series of experiments have been conducted using the VULCAN high power Nd:glass laser at the Central Laser Facility, Rutherford Appleton Laboratory to implement ultra-short pulse operation using the CPA technique. A new target area was commissioned which had a modified target chamber housing one of the compression gratings inside the vacuum vessel and using reflective focusing optics to deliver the pulse to target.

In laser-plasma interaction experiments using the new target facility, we have demonstrated short pulses (~2.4 ps) with energies of ~20 J at focused intensities onto target of ~ 4×10^{17} Wcm^{-2}. A third order cross-correlator was developed for these experiments measuring contrast ratios in the compressed pulse at full output power of ~10^{-6}.

In future experiments it is planned to increase the output power from the facility by using shorter pulses (< 1 ps)[18] and increasing the energy to target to ~ 40 J.

7. ACKNOWLEDGEMENTS

The authors are pleased to acknowledge the valuable assistance of the Optoelectronics Research Centre at Southampton University in the construction of the oscillator.

8. REFERENCES

1. I N Ross et al., "VULCAN - a high-power glass laser for multiuser experiments", IEEE J of QE, QE-17(9), pp 1653-1661, (1981)

2. P Sprangle, E Esarey and A Ting, "Nonlinear interaction of intense laser pulses in plasmas", *Physical Review A*, Vol. 41, No.8, pp 4463-4469, (1990)

3. X F Li, A L'Huillier, M Ferray, LA Lompré and G Mainfray, "Multiple-harmonic generation in rare gases at high laser intensity", *Physical Review A*. Vol. 39, No.11, pp 5751-5761 (1989)

4. P Agostini and G Petite, "Photoelectric effect under strong irradiation", *Contemporary Physics* Vol. 29, No. 1, pp 57-77 (1988)

5. O Willi et al., "Observation of high-density plasmas produced with picosecond high-power KrF irradiation", *Europhysics Letters*, 10(2), pp 141-146, (1989)

6. M M Murmane, H C Kapteyn and R W Falcone, "High-density plasmas produced by ultrafast laser pulses", *Physical Review Letters*, Vol. 62, No. 2, pp 155-158, (1989)

7. D Strickland and G Mourou, "Compression of amplified chirped optical pulse", *Optics Communications*, Vol 56, No 3, pp 219-221 (1985)

8. P Maine, D Strickland and G Mourou, "Tabletop terawatt laser by chirped pulse amplification", SPIE Vol 913 High Intensity Laser-Matter Interactions, pp 140-146, (1988)

9. J M Liu and J K Chee, "Passive mode locking of a cw Nd:YLF laser with a nonlinear external coupled cavity", *Optics Letters*, Vol. 15, No. 12, pp 685-687 (1990)

10. G P A Malcolm, P F Curley and A I Ferguson, "Additive-pulse mode locking of a diode-pumped Nd:YLF laser", *Optics Letters*, Vol. 15, No. 22, pp 1303-1305(1990)

11. RS Grant and W Sibbet, "Cavity configurations for coupled-cavity mode locking", *Optics Communication*, Vol 86, No 2, pp 177-182 (1991)

12. E B Treacy, (Mem. IEEE), "Optical pulse compression with diffraction gratings", *IEEE J of QE*, Vol. QE-5, No. 9, pp 454-458, (1969)

13. O E Martinez, "3000 times grating compressor with positive group velocity dispersion: Application to fiber compensation in 1.3-1.6 μm region", *IEEE J of QE* , Vol. QE-23, No. 1, pp 59-64 (1987)

14. Z Chang et al; CLF annual report, RAL-92-020, Rutherford Appleton Laboratory, UK (1992)

15. Y-H Chuang et al., "Suppression of the pedestal in a chirped-pulse amplification laser", *J Opt Soc Am B*, Vol 8, No 6, pp 1226-1235 (1991)

16. S Luan et al., in press

17. P.A. Norreys et al., to be published.

18. M W Phillips et al., "Self-starting additive-pulse mode-locking of a Nd:LMA laser", *Optics letters*, Vol 17, No20 (1992)